Comparison between simulations and calibrations of a high resolution electrostatic analyzer

J. H. Vilppola[a] and P. J. Tanskanen
Department of Physical Sciences, University of Oulu, P.O. Box 3000, 90401 Oulu, Finland

B. L. Barraclough
Los Alamos National Laboratory, Los Alamos, New Mexico 87545

D. J. McComas
Southwest Research Institute, San Antonio, Texas 78228

(Received 3 November 2000; accepted for publication 13 June 2001)

The ion beam spectrometer (IBS) is one of the three spectrometers in the Cassini plasma spectrometer instrument aboard the Cassini/Huygens spacecraft. The IBS is a very high energy resolution hemispherical electrostatic analyzer. The design values of the IBS are analyzer gap 2.5 mm, and middle radius 100 mm. Because of the high energy resolution required, special care had to be used in the design and manufacturing of the instrument. A simulation was developed in order to aid the designing process. Here we show that the best fit to the laboratory calibration of the IBS flight model is obtained using the simulation model, where the inner hemisphere is misaligned by about 20 μm, where a maximum asymmetry of 75 μm is included in the inner hemisphere, and where the analyzer gap is increased from the design value by about 0.1 mm. We show here that geometric factors postulated in the theoretical model resulted in a better agreement between calibrations and simulations than the geometric factors calculated from calibration data alone. We find a value of $(2.5\pm0.1)\times10^{-4}$ cm^2 sr for the geometric factor of the flight model. Finally, we also show that the energy and angle responses of the IBS are somewhat lower than the values calculated directly from the calibration data: $(2.0\pm0.1)\%$ is the value of the full width at half maximum (FWHM) of the energy distribution, and $(3.1\pm0.1)°$ is the value of the FWHM of the azimuth angle distribution. © *2001 American Institute of Physics.* [DOI: 10.1063/1.1392337]

I. INTRODUCTION

The Cassini/Huygens mission is a joint mission of ESA and NASA, which will investigate the Saturnian system.[1,2] The mission was launched on October 15, 1997. So far Cassini/Huygens has had two gravity assist Venus encounters, one Earth encounter, and one Jupiter encounter. It will arrive at Saturn in July 2004. A short introduction to the Cassini mission can also be found in ''Thesis I.'' [3]

One of the scientific packages aboard the Cassini spacecraft is the Cassini plasma spectrometer (CAPS) investigation,[1,3–5] which consists of three spectrometers: the electron spectrometer (ELS), the ion mass spectrometer (IMS), and the ion beam spectrometer (IBS). ELS is a hemispherical, top hat electrostatic analyzer.[6,7] IMS is a toroidal top hat electrostatic analyzer combined with a linear electric field time of flight spectrometer.[8,9] IBS, which is considered in this article, is a hemispherical electrostatic analyzer. It consists of three entrance aperture–detector pairs. The channel electron multipliers (CEM) are used as detectors.[10] The designed analyzer gap of the IBS is 2.5 mm, and middle radius is 100 mm. CAPS is also equipped with a data processing unit (DPU) and an actuator (ACT), which rotates the instrument.[11]

This study follows up and improves upon our previous work on IBS. Ion orbits inside the analyzer gap between the IBS hemispheres were considered in our first paper, Paper I.[12] In our second paper, Paper II,[13] we studied the effects of stray electric fields on ion trajectories outside of the analyzer. In Paper III[14] we introduced simulations, where asymmetric hemispheres and manufacturing defects were considered. The contents of Papers I–III are collected, combined, and presented in more detail in Thesis I.[3] In this article we focus our attention on the combined effects of manufacturing errors, which could account for unusual transmission properties found during the laboratory calibration of the IBS flight model (IBS-FM). Using an improved simulation code, we attempt to develop a one-to-one correspondence between analytical studies done previously for the spherical section electrostatic analyzer,[15,16] our present simulations, and the calibrations of the IBS. These results can be used, together with the results of Papers I–III, to aid in the design of the high resolution electrostatic analyzers. We show that the magnitude of the errors introduced by manufacturing tolerances is an important consideration when designing new instruments.

In Sec. II of this article we briefly introduce the theory used in our simulations. A much more comprehensive introduction to the algorithm and theory can be found in Papers I–III, or in Thesis I. In Sec. II we also introduce the theory for comparison and analysis of the simulation data and the calibration data. In Sec. III we introduce the latest simulation

[a]Electronic mail: jari.vilppola@oulu.fi

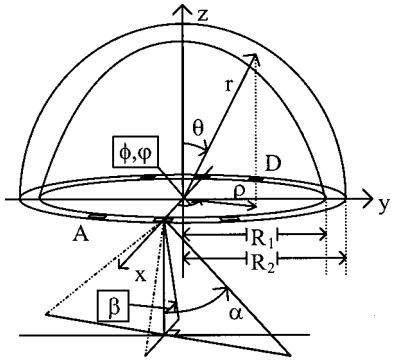

FIG. 1. Coordinate systems (x,y,z), (r,ϕ,θ), and (ρ,φ,z) and angular variables, α and β, used for the initial velocity vector and parameters of the IBS instrument used in the simulations. Later α is also called polar angle and β azimuth angle. The inner radius R_1 is nominally 9.875 cm and outer radius R_2 is 10.125 cm. Letters A and D show a corresponding aperture–detector pair of which there are three. An assumed deformation of the inner hemisphere is schematically shown, and indicates the asymmetric geometry used in the simulations.

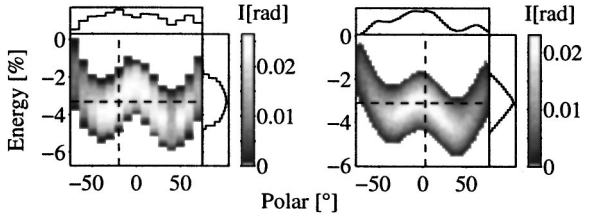

FIG. 2. Two-dimensional energy/polar angle distributions calculated using calibration data (left) and asymmetric simulation data (right). Energy indicates the relative change from nominal energy $[E_{\mathrm{fig}}=(E-E_{\mathrm{nom}})/E_{\mathrm{nom}}*100]$. Intensity, I, gives relative intensity so that the maximum value of the 3D IBS response function is 1. Thus the intensity in the figure gives the number after integration over azimuth angle. In the simulation data the azimuth angle is integrated from $-30.0°$ to $15.0°$, and in the calibration data the azimuth angle is integrated from $-21.6°$ to $14.0°$.

results as well as the results of the laboratory calibration of the IBS-FM. Finally in Sec. IV we discuss our results and speculate on future simulations as well as the possible calibration of the IBS engineering model IBS-EM, which is still available for study.

II. THEORY AND ALGORITHMS

Here we briefly introduce the algorithm used for the detailed studies of ion orbits inside the hemispherical electrostatic analyzer reported in Papers I and III. By using Gauss' law, the electric field E in a spherical condenser can be solved[17] and can be written as

$$E=\frac{\Delta U}{r^2}\left(\frac{R_1R_2}{R_2-R_1}\right), \tag{1}$$

where ΔU is a voltage applied between the hemispheres, r is a distance from the center of the outer hemisphere, R_1 is the radius of the inner hemisphere, and R_2 is the radius of the outer hemisphere. The force is then $F=Eq$, where q is the charge of the ion. If the departure from spherical symmetry is small, as in our case, the central force can be calculated when the distance between the hemispheres, ΔR, is known. First we assume that radius R_2 of the outer hemisphere is constant. Then the radius of the inner hemisphere can be calculated as $R_1=R_2-\Delta R$. Now it is easy to write the equation of motion for the analyzed particles.[18] These differential equations, however, cannot be solved analytically. Therefore the Runge–Kutta algorithm is applied to solve the internal ion orbits numerically.[19]

The ion trajectories outside the analyzer were considered in detail in Paper II. Here we only briefly introduce the algorithm. First the overrelaxation method is used to solve the fringe field in a three-dimensional (3D) cylindrical coordinate system (see Fig. 1) in proximity to the entrance aperture. The 3D equation of motion is then derived and the Runge–Kutta algorithm is again used to solve the equation of motion numerically.[19]

Considerable improvements have been made to our previous work. Referring to the coordinates given in Fig. 1, the asymmetric analyzer geometry used in this article is defined by the following equation:

$$\Delta R_{\mathrm{used}}=\Delta R_{\mathrm{id}}+\Delta R_{\mathrm{ma}}+\Delta R_{\mathrm{as}}[1.33-\cos^2(2\theta)]. \tag{2}$$

Here ΔR_{used} is the gap between the hemispheres. It takes account of any asymmetric hemisphere geometry and misalignments. The parameter ΔR_{id} is the distance between the hemispheres in the ideal IBS instrument (2.5 mm). The parameter ΔR_{ma} gives a correction for the misaligned inner hemisphere (a more detailed definition is given in Paper I). The asymmetry factor ΔR_{as} gives the magnitude of the asymmetry of the inner hemisphere. In the simulations presented here $\Delta R_{\mathrm{id}}=2.5\,\mathrm{mm}$ and $\Delta R_{\mathrm{as}}=75\,\mu\mathrm{m}$. A schematic view of the asymmetric geometry used in the simulations is shown in Fig. 1.

Equation (2) can be used together with Eq. (1) to solve the ion orbits inside the analyzer when an asymmetric inner hemisphere is present. The constant 1.33 shown in Eq. (2) has the effect of making the average distance between the hemispheres in the simulation slightly longer (0.1 mm) than in the ideal instrument. The $\cos^2(2\theta)$ term influences the distance between the hemispheres: the gap is smallest at the top of the analyzer when the polar angle is 0.0° and greatest when the polar angle is 45.0°. Thus ions entering the aperture at 0° polar angle see, on the average, a narrower gap between the hemispheres, and therefore experience a stronger electric field than ions entering at a 45.0° polar angle. In order to transit the analyzer, particles with 0° polar angle (also $\geqslant$60.0°) need more energy. When all of these effects are considered a double-curved energy versus polar angle distribution results (Fig. 2). This distribution is strikingly similar to the distribution measured in the laboratory during IBS-FM calibrations.

Using the given geometry, one can simulate the operation of the IBS instrument. Our simulation routine produces a 3D data matrix, where the individual value represents the number of ions transmitted for various ion beam entrance angles relative to the aperture. The beam position is defined by the polar and azimuth angles and the central energy of the ion beam. The ion beam variation in our simulation can be found in Table I. The resulting 3D data matrix is called the IBS response function.

TABLE I. Laboratory ion beam properties for different simulation configurations. The relative energy variation dE/E and combined angular variation d(angle) are given for each configuration.

Geometry	dE/E (%)	d(angle) (°)
Ideal simulation[a]	±0.06	±0.1
Asymmetric simulation[b]	±0.06	±0.1
Ion beam simulation[c]	±1.0	±0.5

[a]The design values are used for all IBS parameters and the values for the laboratory ion beam simulation are the same as in Paper II.
[b]The same as footnote a but with an asymmetric inner hemisphere with a 75 μm asymmetric factor and a misalignment in the y direction (15 μm) and in the z direction (-10 μm).
[c]The same as footnote b but now the laboratory ion beam has been simulated with larger deviations.

A similar data matrix was also obtained by using laboratory calibration data. In the calibration we measured numerous two-dimensional cuts through the IBS response function. First, the maximum of the IBS response function was found. Second, we measured the central cuts, where two of the variables varied and one was kept constant, yielding an energy/polar distribution with constant azimuth angle, an energy/azimuth distribution with constant polar angle, and an azimuth/polar distribution with constant energy. The next step was to determine other two-dimensional (2D) distributions and construct the full 3D IBS response function.

For the calibration of the IBS flight model, we set the polar angle to be constant during the measurements of various energy/azimuth scans. The result was an energy/azimuth distribution at numerous polar angles. Since the ion beam conditions might have varied during laboratory calibrations, which were executed over several days, the central energy/polar cut with constant azimuth angle was used to normalize various data accumulations. It is assumed that ion beam conditions were sufficiently steady over the period of time required to measure each 2D distribution. Normalization is done for each energy/azimuth distribution with constant polar angle using several points along the cut line of two planes defined by the energy/azimuth distribution with constant polar angle, and the normalizing energy/polar distribution with constant energy. The error due to random noise was minimized using several points instead of one single point.

For each data point in the IBS response function we applied an appropriate dead time correction to the counts. The dead time is the minimum amount of time that must separate two events for both events to be detected. The correction is given by

$$c_T = \frac{c_M}{1 - c_M T_{\mathrm{dt}}}, \tag{3}$$

where c_T is the true counts per second, c_M is the measured counts per second, and T_{dt} is the detector dead time.

The geometric factor G of the hemispherical electrostatic analyzer can be calculated using the formula

$$G = [A]\left[\left\langle \Delta\beta \frac{\Delta E}{E} \right\rangle \int_{\Delta\alpha}\right], \tag{4}$$

where

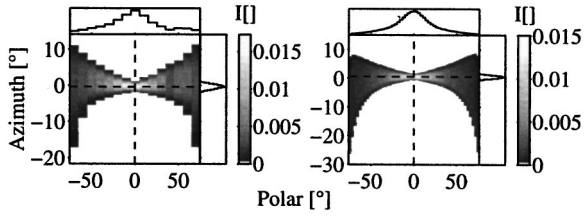

FIG. 3. Two-dimensional azimuth/polar distributions calculated from calibration data (left) and asymmetric simulation data (right). Symbols in the figure are defined as in Fig. 2. In the simulation data the relative energy is integrated from -6.0% to 0.0% and in the calibration data from -6.628% to 0.195%.

$$\left\langle \Delta\beta \frac{\Delta E}{E} \right\rangle \int_{\Delta\alpha} = \frac{\Sigma_{ijk} C_{ijk} \delta E_i \delta\beta_j \delta\alpha_k \cos\alpha}{\max(C_{ijk})}. \tag{5}$$

In Eq. (4), A is the area of the entrance aperture, which can be calculated when the width and the length of the aperture is known. In the IBS-FM this number is 37.5 mm^2 ($=2.5 \times 15$ mm^2). The integration given in Eq. (5) implies an integration over the IBS response function in both angle and relative energy. In the discrete sum, where the IBS response function is integrated over energy and azimuthal and polar angles, C_{ijk} gives the counts for each ion beam position, δE_i gives the bin width in energy, $\delta\beta_j$ in azimuthal angle and $\delta\alpha_k$ in polar angle. When the geometric factor is calculated using formulas (4) and (5) the detector efficiency is assumed to be 100%. The laboratory calibration data were renormalized to 100% detector efficiency and hence all numbers given in this article are comparable with each other.

Note that the definition of the angles used in our previous simulations was somewhat misleading. In principle, the rotation axis of the polar and azimuth angles should be in the aperture plane. The polar angle in Papers I–III conforms with this but the azimuth angle used does not. In this article, however, the angle definitions conform with this rule. Because of the curved entrance aperture the polar and azimuth angles are mixed especially for large polar angles. This causes the so-called ''butterfly effect'' in the azimuth versus polar angle distribution (Fig. 3). Since the angles were defined differently in this article from the definition in our previous papers, the butterfly effect also appears differently in the azimuth versus polar angle distribution. Thus the butterfly shaped distribution function given by Eqs. (3a) and (3b) and by Fig. 9 in Paper II must be used with special care if compared with the similar corresponding distribution in this article. The magnitude of the butterfly effect is underestimated when the definitions of Paper II are used. The situation is the same in all figures, where the azimuth angle is present, except the ones where a central cut for polar angle is used. The butterfly effect is also considered elsewhere[15,16] using the same angle definitions as used in this article.

III. RESULTS

The simulations presented here were calculated using the same code as in our previous papers. In Papers I and II the effect of misaligned ideal hemispheres was discussed, and in Paper III the effect of an asymmetric inner hemisphere was studied. In this study a final geometric error is introduced

yielding the best fit to calibrations. The assumed asymmetry for the inner hemisphere is defined in Eq. (2). This inner asymmetric hemisphere was moved along the main coordinate axis, defined in Fig. 1, with respect to the ideal outer hemisphere. The misalignment used was $dx=0\ \mu$m, $dy=15\ \mu$m, and $dz=-10\ \mu$m. These numbers were selected because the energy/polar distribution of the calibration is rotated and curved slightly (Fig. 2). In Paper II we proved that misalignment in the positive z direction curves the energy/polar distribution, since on the average the particle encounters a narrower gap and thereby a stronger electric field when its polar angle is close to zero at the entrance aperture. In Paper II we also proved that misalignment in the positive y direction rotates the energy/polar distribution. Now particles with large negative polar angles at the entrance aperture encounter a stronger electric field than particles with large positive polar angles. When these results are used it is obvious that the misalignments given above are the most reasonable ones. This can be verified by comparing the energy/polar distributions given for calibration and selected simulation configurations in Fig. 2.

The simulation configuration described above is later referred to as the ''asymmetric simulation.'' The ideal IBS instrument was also simulated and some results are given in this article and are referred to as the ''ideal simulation.'' Larger energy and angle deviations of the simulated laboratory ion beam were also studied. These results are referred to as the ''ion beam simulation.'' More details about the simulation configuration studied in this article can be found in Table I. If not otherwise noted, the simulation results are obtained using the asymmetric simulation definition given in Table I.

Because of the angle definition, the azimuth angle deviation shown here is larger than that shown in our previous simulations. Here, the azimuthal angle is varied from $-30°$ to 15° in steps of 0.2° (226 steps). The relative energy is varied from -6.0% to 0.0% in steps of 0.12% from the nominal value (51 steps). The nominal energy gives the energy of a proton which has a circular orbit in the middle of the analyzer gap of an ideal instrument. The nominal energy is equal to 0% relative energy. Since the asymmetric simulation configuration differs from the ideal simulation configuration, all energies are lower than the nominal energy in the ideal instrument. In the simulations, the polar angle varies from $-75°$ to 75° in 3.0° steps (51 steps). From each parameter combination the calibration ion beam was simulated using 10^5 particles. In Paper II the ion beam parameters are defined more precisely. Only those ions which transited through the analyzer were counted. As a result a 3D IBS response function was obtained from which all simulation figures were calculated.

When considering the IBS-FM calibrations, we used the method described in Sec. II. The polar angle values were $\alpha=-70°,-60°,\ldots,60°,70°$. From each of these polar angles one 2D energy/azimuth cut was measured. Thus we obtained a counting frequency as a function of energy and azimuth angle. A wider azimuthal response was obtained for large polar angles (the ''butterfly'' effect). When the 3D IBS response function was calculated from the calibration data,

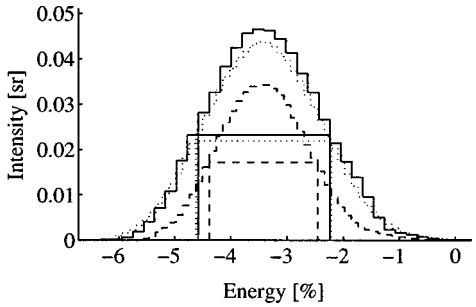

FIG. 4. One-dimensional energy distributions. The solid line gives the distribution calculated from the calibration results, the dashed line from the asymmetric simulation results, and the dotted line from ion beam simulation results (see Table I). Energy is the same as in Fig. 2, where the relative intensity is also defined. It gives the number after integration over azimuth and polar angles. In the simulation data the polar angle is integrated from $-75.0°$ to 75.0° and in the calibration data from $-70.0°$ to 70.0°. The integration limits of the azimuth angle are given in Fig. 2.

points were interpolated for azimuth angles that were not directly measured. Basically, the energy/azimuth distribution for a polar angle $\alpha=0.0°$ defines the steps used in energy and azimuthal angle since the steps are smallest in that distribution. In the calibration, energy deviations are evaluated by varying the plate voltage between the hemispheres instead of varying the beam energy. The voltage was stepped from 512 to 547 V in steps of 1.0 V. A lower voltage is equivalent to a higher energy. In our calibration the measured beam energy at the ion source was 10 006 eV. In an ideal instrument the entrance fringe field accelerates ions of this energy from 0 V potential at infinity into the 253.3 V potential at the middle of the analyzer gap. Thus in an ideal instrument the energy for a particle entering the analyzer in the center of the aperture is 10 259.3 eV. An ion with this energy will exactly transit the center of the ideal analyzer gap when -513.0 V is applied to the inner hemisphere and the outer hemisphere is grounded. Using -513.0 V as a nominal plate voltage, the relative deviations from the nominal value can be calculated. Basically it makes no difference whether the calculations or calibrations were executed keeping the inner hemisphere at a constant potential and allowing the ion beam energy to vary. This fact was confirmed by using both methods in our simulation model, and the corresponding distributions were found to be similar. Hence it is reasonable to conclude that the energy was varied from -6.628% to 0.1949% in steps of 0.1949%. The azimuthal angle was varied from $-21.6°$ to 14.0° in steps of 0.20°.

One-dimensional normalized energy distributions calculated from the simulation data of the asymmetric and ion beam simulation configurations and the laboratory calibration data are given in Fig. 4. In order to avoid random noise variations in all simulations the maximum response value was first found by simulating several points near the maximum of the IBS response function by repeating the simulation at each point 100 times. The averages were then calculated for each of these points and the maximum average was defined to be the maximum of the IBS response function. For better statistics the simulation was repeated 1000 times at this maximum point. After normalization the angles were integrated to yield the intensity as a function of energy. One-

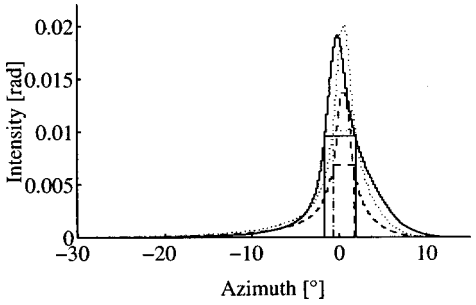

FIG. 5. One-dimensional azimuth angle distributions. The solid line is the calibration result, the dashed line the asymmetric simulation result, and the dotted line the ion beam simulation result (see Table I). Intensity in the figure gives the relative intensity as in Fig. 4. The integration limits of energy are given in Fig. 3 and the polar angle is integrated as described in Fig. 4.

dimensional azimuth angle distributions calculated from the same simulations and calibration data are given in Fig. 5, and one-dimensional polar angle distributions are given in Fig. 6. Finally the geometric factor [Eq. (4)] can be calculated by integrating over these distributions and multiplying by the entrance aperture area.

Two-dimensional distributions were also calculated from the IBS response functions. The differences are discussed below (see Sec. IV). The energy versus polar angle distribution calculated from the calibration data and the asymmetric simulation data are given in Fig. 2. In the calculations the IBS response functions were first normalized to the maximum as described in the previous section. Next, the fixed parameter was integrated over the whole range. The normalized intensity is in radians if the fixed parameter is an angle and it is dimensionless if the fixed parameter is relative energy. By integrating over both variable parameters in the distributions and then multiplying the value with the area of the entrance aperture we again find the same geometric factor as defined in Eq. (4). The energy/azimuth distribution for the calibration data and the asymmetric simulation data are given in Fig. 7, and the azimuth/polar distributions are given in Fig. 3.

In Paper II we also gave distributions, called cuts, where the fixed parameter was held constant. Since energy/polar distributions at constant central azimuthal angles resemble

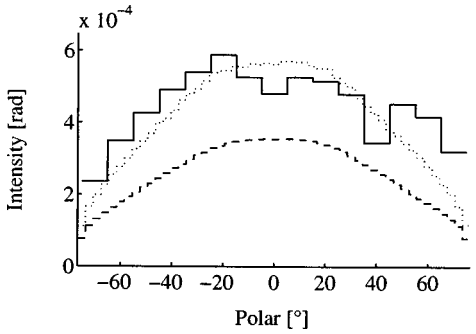

FIG. 6. One-dimensional polar angle distributions. The solid line is the calibration result, the dashed line the asymmetric simulation result, and the dotted line the ion beam simulation result (see Table I). Intensity in the figure gives the relative intensity as in Figs. 4 and 5. The azimuth angle and relative energy are now integrated and the polar angle is not. Integration limits can be found in the figure captions of Figs. 2 and 3.

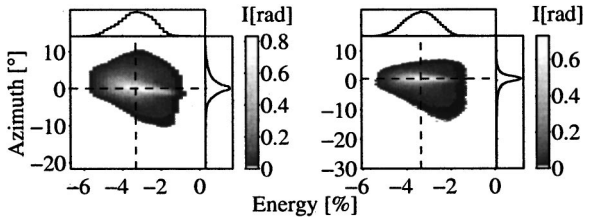

FIG. 7. Two-dimensional energy/azimuth distributions calculated using calibration data (left) and asymmetric simulation data (right). Symbols in the figure are defined as in Fig. 2. The polar angle integration limits are given in Fig. 4.

the distributions where the azimuth angle was integrated over the entire range, they are not shown here. The main difference between these distributions is that the full width of half maximum (FWHM) area is more localized to the near zero polar angle values. This is a result of the butterfly effect which spreads the azimuth distribution for large polar angles, and much lower intensities are obtained. When considering the azimuth polar angle distributions at a constant central energy it is clear that since the butterfly effect is almost independent of energy variations, there is not much difference in the distribution when energy is integrated over the entire range. Thus these distributions are not shown here. In the energy/azimuth distribution, (Fig. 7) integration over polar angle results in a wider distribution in azimuth angle than the distribution where the polar angle has had a constant zero value. Also, the double curved shape of the energy/polar distribution causes a wider energy scale when the polar angle is integrated over the whole scale. Thus we introduce the energy/azimuth distributions with polar angle $\alpha = 0.0°$. The distribution calculated using the calibration data and the asymmetric simulation data are shown in Fig. 8.

The FWHM values of the 1D energy and azimuth angle distributions were defined using the corresponding 1D distributions, and are given, along with the geometric factors, in Table II. In this table we also give the value of the theoretical geometric factor and the FWHM values of the 1D energy and azimuth distributions calculated for the IBS instrument with ideal geometry using design values for all parameters[15] (ideal theoretical), and with those values for parameters which yield closest fit with the IBS laboratory measurements (lab theoretical). These values indicate that the actual radius of the inner hemisphere, R_1, is 9.870 cm (ideal = 9.875 cm) and the outer radius, R_2, is 10.130 cm (ideal = 10.125 cm), and that the gap between the plates, ΔR, is 2.60 mm (ideal = 2.50 mm), and a center radius, R_{mid}, is 10.000 cm.

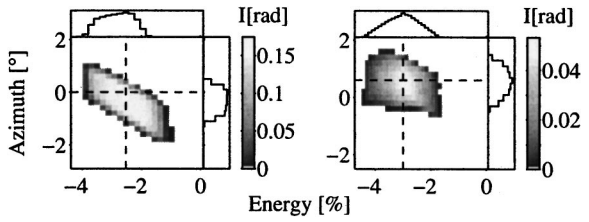

FIG. 8. Two-dimensional energy/azimuth distribution calculated from calibration data (left) and asymmetric simulation data (right). The symbols are defined as described in Fig. 2. The data have been integrated over one single bin in polar angle.

TABLE II. The FWHM values of the 1D energy and azimuth distributions of the calibration data, some simulation data, and the theoretical calculations. Also given are the geometric factors calculated from calibration data, using theoretical models and calculated from some simulated configurations. The simulation configurations are explained in more detail in Table I. The error limits of the given FWHM values are the bin widths used in corresponding distributions. The given errors are 95% confidence limits when considering the geometric factors of the simulations. The error limit of the geometric factor of the calibration gives the error defined directly from the data.

Geometry	FWHM $\Delta E/E$ (%)	FWHM $\Delta\beta$ (°)	Geometric factor (cm^2 sr)
Calibration	2.5 ± 0.2	3.6 ± 0.2	$(4.32\pm0.08)\times10^{-4}$
Ideal theoretical	1.31	2.05	2.02×10^{-4}
Lab theoretical	1.37	2.13	2.27×10^{-4}
Ideal simulation	1.52 ± 0.12	2.3 ± 0.2	$(2.413\pm0.011)\times10^{-4}$
Asymmetric simulation	1.93 ± 0.12	2.3 ± 0.2	$(2.596\pm0.012)\times10^{-4}$
Ion beam simulation	2.42 ± 0.12	2.7 ± 0.2	$(4.13\pm0.09)\times10^{-4}$

IV. DISCUSSION

Although the calibration results and the simulation results using the asymmetric simulation configuration are quite similar, there are still some differences which should be considered. From Fig. 4 where the 1D energy distributions are given, it can be seen that the maximum intensity in all three distributions occurs for the same energy value -3.4%. This means that in general the gap between the hemispheres in the instrument is somewhat larger than the design value. The most notable difference is in the width of the distributions. While the simulation (asymmetric simulation configuration) gives about 1.9% FWHM, the calibration gives about 2.5% FWHM (See Table II). One may explain the larger FWHM value by arguing that the actual gap between the analyzer plates may be larger. This explanation can be ruled out by comparing the ion beam energy and the voltage on the inner hemisphere. The ratio between specific ion beam energy and plate voltage is related to the analyzer gap. Thus a wider gap gives a different ratio. In Fig. 4 comparison of the simulation and calibration results show that these three parameters are similar, and the result is a wider energy distribution in the calibration than in the simulation.

When considering the energy distributions with constant polar angles as given by Fig. 2 one may notice that for each polar angle value the calibration data gives a wider distribution than for the simulation, but not as wide as the energy distribution given in Fig. 4 where the 1D energy distribution is shown. Thus one can expect a wider 1D integrated energy distribution despite the double curved shape of the 2D energy/polar distribution. As can be seen in Fig. 2, the double curved shape is quite similar in both distributions and yields wider distributions in both cases. The size of this effect can be estimated by comparing the FWHM values of the ideal simulation and asymmetric simulation given by Table II. In the simulations the double curved effect increases the FWHM value of the integrated 1D energy distribution by about 0.4%, from 1.5% to 1.9%. However, there is still a notable difference between the 2D energy/polar distributions of the calibration and the asymmetric simulation configuration. The simulation figure behaves as expected and gives a lower intensity at large polar angles, while in the calibration figure the intensity remains higher and drops much later with increasing polar angle. Thus the calibration figure intensity is approximately the same at the curved area where the polar angle is about $\pm40°$ while in the simulation figure the intensity has already started to fall because of the cosine effect in the polar angle. This effect widens the 1D integrated energy distribution of the calibration with respect to the simulation distribution.

The difference between the calibration data and the simulation data can be confirmed by comparing the 1D polar angle distributions given in Fig. 6. The ion beam simulation gives a cosine-like distribution while the calibration distribution is much flatter at the top of the distribution. One may also notice the random noise-like behavior between neighboring bins in the calibration distribution as well as the asymmetric shape of the distribution. However, the statistics of the calibration are very good, and thus the distributions should behave even more smoothly than in the simulations. It is possible that laboratory ion beam intensity variations may have occurred during the measurement of a single energy/polar data file (less than 1 h), which was used as a normalizer for several energy/azimuthal data files as described in Sec. II. The required variation in the intensity is about 20% which could explain the random noise-like behavior of the polar angle distribution. Another possibility would be that the intensity remained constant, but while rotating the IBS-FM in the chamber, the aperture did not remain in the middle of the beam during the entire time, or the beam was not uniform. However, when considering the laboratory conditions, both of these explanations are unlikely. Alternatively, if the reason is intrinsic to the IBS instrument itself, it could either be in the hemispherical sensor or in the CEM detectors. At some polar angles the hemispheres may be dented (a few to a few 10s of μm) causing the reduced transmission intensity at the detector end of the sensor. Another possibility could be that the hemispheres are deformed in a such way that the transmitted ion beam does not face the target detector properly. This tangential field acceleration has not been studied in our simulation model. A third alternative is that the CEM detector is polar angle sensitive. In that case, the flat top of the 1D polar distribution may be a reasonable result. Thus it can be concluded that the simulation geometry must somehow be different from the real geometry of the IBS-FM sensor. Since there are several possible explanations, which can be cumulative or even cancel each other, additional measurements are required. These can be done in a laboratory using the IBS-EM.

As mentioned in the previous paragraph the nominal energy, plate voltage, and the gap between the hemispheres are intimately related to one another. Because of this, a different explanation for the wider energy distribution at a constant polar angle in the calibration data is needed. Here we have shown that the simulations and theoretical models are consistent with each other. Therefore the reason for the wider energy distribution in the calibration data lies somewhere else. One candidate is a wider energy deviation in the ion beam energy as suggested by the simulated 1D energy distribution (Fig. 4). By increasing the ion beam energy deviation the energy distribution becomes wider (see Tables I and II): at 2.4%, it is much closer to the calibration value than the value given by the asymmetric simulation model. When considering the simulations, it can be assumed that since a wider deviation in the laboratory ion beam increases the FWHM of the energy distribution by about 0.5%, there is a similar overestimation in the calibration results as well. Thus it can be concluded that the value of the FWHM of the energy distribution given by Table II is too high. The true value of the IBS-FM should then be in the neighborhood of $(2.0 \pm 0.1)\%$.

When considering all three 1D azimuth angle distributions given in Fig. 5, it is clear that the calibration gives the widest FWHM value (See Table II). A comparison between the two simulation configurations shows that the wider energy and angle deviation in the simulated laboratory ion beam also produces a wider distribution. Thus one reason for the wider azimuth angle distribution of the calibration has been accounted for. Another aspect can be found by considering the 1D polar distributions and 2D azimuth/polar distributions given by Figs. 3 and 6. The intensity of the 1D polar distribution is too high at the larger polar angles, and higher intensity is present where the butterfly effect spreads the deviation of the azimuth angle. These particles can also be seen as a broader distribution in the 1D integrated azimuth plot. Other aspects in 1D azimuth distributions and 2D azimuth/polar distributions are also closely correlated. Table II shows that the ideal and asymmetric simulation configurations give exactly the same FWHM value for the integrated azimuth angle distribution. After the wide deviations in laboratory, ion beam has been included in the simulation model, the FWHM value of the azimuth angle distribution increases about 0.4° from 2.3° to 2.7°. Thus the real FWHM value of the calibration is probably lower than the one given in Table II. As a result we give $(3.1 \pm 0.1)°$ as an estimation for the actual value. If the flat top of the 1D polar distribution is an artifact caused by calibration conditions, this number would still be too high.

The 2D energy/azimuth distributions given in Figs. 7 and 8 are basically in good agreement with each other. Because of great similarity between the 2D distributions obtained from the ion beam simulation and the ideal simulation, figures are not given here. The only notable difference is again a wider distribution in relative energy direction, as discussed above. When only the width of the distribution in energy direction is considered, the ion beam configuration gives distributions which are closer to the calibration results than results given by asymmetric simulation.

When comparing the geometric factors (Table II), the ion beam simulation configuration yields almost the same value as the calibration. If the energy and the angle deviations are increased, as discussed above, we would also have larger geometric factors. Using the narrow deviation simulation (asymmetric and ideal simulation) models, almost the same value for the geometric factor has been obtained as was calculated using theoretical models for spherical section electrostatic analysers. Thus it appears that the geometric factor from the calibration is overestimated. It seems likely that the entire difference between the geometric factors of the calibration and the narrow deviation simulations are not caused entirely by real effects in the IBS-FM, but rather by the properties of the laboratory ion beam, which are not well known. Following the discussion given above we conclude that the best choice of the geometric factor is somewhere near the theoretical calculations and simulations with a narrow laboratory ion beam, around $(2.5 \pm 0.1) \times 10^{-4}\ \mathrm{cm^2\,sr}$. This assumption may have to be corrected if evidence is found that the transmission properties differ substantially from the simulations and theoretical model.

In this study we have found that almost all differences between the shape of the distributions between the calibration and simulations can be understood. Since the simulation model, where asymmetric hemisphere geometry is present, yields a similar double curved distribution as measured in the laboratory calibration of the IBS-FM, it can be assumed that something similar in the geometry of the hemispheres might cause the observed effect of the IBS-FM. Some of the arguments given above also suggest that the real geometry of the IBS-FM differs somewhat from the geometry used in our simulations. However, our simulation results give guidelines for the scale of the geometric errors in the actual instrument. When the knowledge of the simulation and laboratory calibration is combined, it can be concluded that the energy resolution of the IBS-FM is $(2.0 \pm 0.1)\%$ (FWHM value), the angular resolution is $(3.1 \pm 0.1)°$ (FWHM value), and finally that the geometric factor is $(2.5 \pm 0.1) \times 10^{-4}\ \mathrm{cm^2\,sr}$.

ACKNOWLEDGMENTS

The authors would like to acknowledge the University of Oulu and the Academy of Finland for financial support of this project. Work at Los Alamos was carried out under auspices of the U.S. Department of Energy with support from NASA under the Cassini project.

[1] NASA, A Proposal for the Plasma Science (PLS) Investigation for the Cassini Orbiter Spacecraft, Volume 1: Investigation and Technical Plan, SwRI Proposal 15-9376.
[2] Announcement of Opportunity, Cassini Mission: Huygens Probe, ESA REF SCI(89)2, (1989).
[3] J. H. Vilppola, Licentiate thesis: Cassini Mission and the CAPS/IBS Instrum, University of Oulu, 1998 (this thesis can be accessed in pdf format at http://spaceweb.oulu.fi/~jari/).
[4] D. T. Young, B. L. Barraclough, J. J. Berthelier, M. Blanc, J. L. Burch, A. J. Coates, R. Goldstein, M. Grande, T. W. Hill, J. M. Illiano, M. A. Johnson, R. E. Johnson, R. A. Baragiola, V. Kelhä, D. Linder, D. J. McComas, B. T. Narheim, J. E. Nordholt, A. Preece, E. C. Sittler, K. R. Svenes, S. Szalai, K. Szegö, P. Tanskanen, and K. Viherkanto, Proc. SPIE **2803**, 118 (1996).
[5] D. T. Young, B. L. Barraclough, J. J. Berthelier, M. Blanc, J. L. Burch, A.

J. Coates, R. Goldstein, M. Grande, T. W. Hill, J. M. Illiano, M. A. Johnson, R. E. Johnson, R. A. Baragiola, V. Kelha, D. Linder, D. J. McComas, B. T. Narheim, J. E. Nordholt, A. Preece, E. C. Sittler, Jr., K. R. Svenes, S. Szalai, K. Szeg, P. Tanskanen, and K. Viherkanto, AGU Monograph **102**, 237 (1998).

[6] A. J. Coates, C. Alsop, A. J. Coker, D. R. Linder, A. D. Johnstone, R. D. Woodliffe, M. Grande, A. Preece, S. Burge, D. S. Hall, B. Narheim, K. Svenes, D. T. Young, J. R. Sharber, and J. R. Scherrer, J. Br. Interplanet. Soc. **45**, 387 (1992).

[7] D. R. Linder, A. J. Coates, R. D. Woodliffe, C. Alsop, A. D. Johnstone, M. Grande, A. Preece, B. Narheim, K. Svenes, and D. T. Young, AGU Monograph **102**, 257 (1998).

[8] D. J. McComas, J. E. Nordholt, J.-J. Berthelier, J. M. Illiano, and D. T. Young, AGU Monograph **102**, 187 (1998).

[9] J. E. Nordholt, J. J. Berthelier, D. M. Burr, H. O. Funsten, D. J. McComas, D. M. Potter, K. P. McCabe, J. M. Illiano, D. T. Young, and R. Goldstein, AGU Monograph **102**, 209 (1998).

[10] D. J. McComas, J. R. Baldonado, S. J. Bame, and B. L. Barraclough, Rev. Sci. Instrum. **58**, 2331 (1987).

[11] T. Ylikorpi *et al.*, Development of an Actuator for CAPS Instrument on Spacecraft Cassini, ESA SP-374, 97–101 (1995).

[12] J. H. Vilppola, J. T. Keisala, P. J. Tanskanen, and H. Huomo, Rev. Sci. Instrum. **64**, 2190 (1993).

[13] J. H. Vilppola, P. J. Tanskanen, H. Huomo, and B. L. Barraclough, Rev. Sci. Instrum. **67**, 1494 (1996).

[14] J. H. Vilppola, P. J. Tanskanen, and B. L. Barraclough, *Proceedings of the Ninth COSPAR Colloquim, Beijing, China, 1996* (Elsevier Science, Oxford, England, 1998), Vol. 9, pp. 75–84.

[15] J. T. Gosling, M. F. Thomsen, and R. C. Anderson, Los Alamos National Laboratory Report No. LA-12962-MS, 1984 (unpublished).

[16] J. T. Gosling, J. R. Asbridge, S. J. Bame, and W. C. Feldman, Rev. Sci. Instrum. **49**, 1260 (1978).

[17] I. S. Grant and W. R. Phillips, *Electromagnetism* (Wiley, New York, 1976).

[18] M. R. Spiegel, Theory and *Problems of Vector Analysis and an Introduction to Tensor Analysis* (McGraw-Hill, New York, 1959).

[19] W. H. Press, B. P. Flannery, S. A. Teukolsky, and W. T. Vetterling, *Numerical Recipes, The Art of Scientific Computing* (Cambridge University, Cambridge, England, 1986).